Random fields and orientational order in $Rb(CN)_xBr_{1-x}$ mixed crystals: A study of static-shear elasticity

J. O. Fossum, A. Wells, and C. W. Garland
Department of Chemistry and The Center for Materials Science and Engineering, Massachusetts Institute of Technology, Cambridge, Massachusetts 02139
(Received 4 December 1987)

Ultrasonic measurements of static c_{44} shear elastic constants in $Rb(CN)_xBr_{1-x}$ single crystals are presented. The data are analyzed using a mean-field model which includes quenched random strain fields, accounting for systematic deviations from a simple Curie-Weiss equation. The agreement between theory and experimental data is excellent. The Edwards-Anderson order parameter q falls off as $1/T^2$ at high temperatures, in agreement with the high-temperature-expansion result. At low temperatures the behavior of q is analyzed using a low-temperature expansion. The present data and analysis provide strong support for the idea that the glassy states in mixed cyanide systems are of random-field rather than random-interaction nature.

I. INTRODUCTION

At room temperature pure rubidium cyanide and mixed crystals of $Rb(CN)_xBr_{1-x}$ $(0<x<1)$ possess time-averaged pseudocubic rocksalt structures ($Fm3m$), where the dumbbell-shaped CN^- ions jump rapidly between orientational local-potential minima.[1] A physically crucial factor in these crystals, and in other mixed cyanide systems (KCN_xBr_{1-x}, $K_xRb_{1-x}CN$, $K_xNa_{1-x}CN$, etc.) is the strong coupling between cyanide rotational degrees of freedom and lattice strains, both of quadrupolar symmetry.[1,2] This so-called translational-rotational (TR) coupling gives rise to a strong lattice-mediated CN^--CN^- coupling that triggers a first-order elastic phase transition on cooling the pure materials KCN, NaCN, and RbCN. At these transitions the cyanide orientations of quadrupolar (T_{2g}) symmetry and the lattice strains freeze out simultaneously,[3] giving a monoclinic low-temperature phase in the case of pure RbCN.[1,4] The most dramatic effect of this TR coupling is the soft-mode behavior of the c_{44} elastic constants on cooling prior to the first-order elastic transitions.[5,6]

There is no electric-dipolar, i.e., head to tail, ordering of the cyanide ions occurring at the elastic transitions.[1,7] Electric-dipolar freezing does occur in most mixed cyanide crystals at temperatures below the quadrupolar freezing, but no long-range electric-dipolar ordering occurs in RbCN.[8] The bulk of recent research on mixed cyanide systems has focussed on the quadrupolar (elastic) ordered phases and quadrupolar glassy phases.[1,9] In the latter cases it has been proposed that long-range quadrupolar order is destroyed due to random quenched strains induced by the difference in ionic radii between the substitutional ions.[10,11] Thus, it has been suggested that the low-temperature state of mixed cyanide crystals can be understood in terms of two competing effects—the lattice-mediated CN-CN coupling and quenched random strain fields.

A recent theory for mixed crystals by Michel,[10,11] proposes a modified static susceptibility in which the random quenched strains are included in terms of a lowest-order high-temperature series correction to the underlying mean-field Curie-Weiss law. This explains the static systematic deviations from simple Curie-Weiss behavior observed below the critical composition x_c in diluted cyanide mixtures. x_c is the composition below which the crystals stay cubic down to the lowest temperatures;[12] for the present system, the value $x_c \simeq 0.58$ has been estimated on the basis of optical studies.[13] These ideas have only very recently been experimentally verified.[14] In a recent letter, where we reported data analysis of c_{44} elastic constants in $K(CN)_xBr_{1-x}$, $K(CN)_xCl_{1-x}$, and $Rb(CN)_xBr_{1-x}$ crystals,[14] we showed that the quenched random strain model accounts successfully at least for the high-temperature static behavior of the elastic constants, and that an extended formalism including low-temperature expansion in the random fields possibly can account for the static behavior at low temperatures.

The present work involves measurements of the TA [100] acoustic velocities in the cubic high-temperature phase of eight different mixed $Rb(CN)_xBr_{1-x}$ single crystals. The static elastic-constant data are well represented by a modified mean-field Curie-Weiss equation that includes a contribution from a random conjugate-field-induced Edwards-Anderson order parameter. The fits to the data yield extrapolated second-order transition temperatures that follow mean-field percolation theory and random-field distribution widths that are in complete agreement with theoretical predictions.

In Sec. II, we will summarize some relevant assumptions and ingredients underlying the random strain field model. The experimental procedures and results are described in Sec. III, and a detailed discussion of data analysis and interpretation is given in Sec. IV. In Sec. V we make some concluding remarks.

II. REVIEW OF THEORY

We present here a mean-field theory for calculating the behavior of the static elastic constants in cyanide sys-

tems. Our basic assumptions about the physics involved in the problem are completely analogous to assumptions made by Michel[10,11] in his mean-field treatment of a microscopic model for mixed $A(CN)_xX_{1-x}$ crystals. Our approach differs from Michel's in one aspect, however. Instead of starting from a microscopic model and extracting the thermodynamics with a mean-field approximation at the end, we assume mean-field theory to be valid at the very beginning.

The lowest-order Landau expansion of the free energy per unit volume for a given ACN sample in the cubic *high-temperature phase* thus reads

$$F=F_0+\tfrac{1}{2}\alpha(T-T_0)Y^2+\gamma Y\epsilon_4+\tfrac{1}{2}c_{44}^0\epsilon_4^2 , \tag{1}$$

where T is the temperature and Y is the relevant cyanide orientational order parameter, a macroscopic rotational parameter of quadrupolar symmetry. Note that there is a bilinear coupling with coupling strength γ present between Y and the shear strain ϵ_4. It is essential to the physics of the present problem that the bilinear coupling is strong, i.e., the third term in Eq. (1) is energetically the most important one at low enough temperature. The coefficients α and γ are assumed to be independent of T. The bare elastic constant c_{44}^0 is expected to exhibit a weak x dependence due to small changes in the cubic lattice parameter and a very weak T dependence due to crystal anharmonicity.[15–17]

The elastic constant c_{44}^0 represents the elastic stiffness one would observe in the absence of bilinear coupling (i.e., $\gamma=0$). T_0 is the temperature at which cyanide ions would undergo quadrupolar order in the absence of bilinear coupling, and α^{-1} is the Curie constant for such an uncoupled system.

By minimizing F with respect to the order parameter Y (or the strain ϵ_4), one obtains a relation between Y and ϵ_4, which allows one to rewrite Eq. (1) in the form

$$F=F_0+\tfrac{1}{2}c_{44}\epsilon_4^2 , \tag{2}$$

where the elastic constant c_{44} is given by

$$c_{44}=c_{44}^0-\frac{\gamma^2}{\alpha}\frac{1}{T-T_0} . \tag{3a}$$

In terms of the elastic compliance s_{44}, this becomes

$$s_{44}\equiv\frac{1}{c_{44}}=s_{44}^0\frac{T-T_0}{T-T_c}=s_{44}^0\left[1+\frac{T_c-T_0}{T-T_c}\right] . \tag{3b}$$

Both Eqs. (3a) and (3b) represent elastic Curie-Weiss laws. In Eq. (3b) $s_{44}^0=1/c_{44}^0$, and $T_c=T_0+\gamma^2/\alpha s_{44}^0$. A more general form for the compliance is

$$s_{44}=s_{44}^0(1+\beta\chi) , \tag{4}$$

where χ is the dimensionless order parameter susceptibility. For the Landau model described above, χ is given by

$$\chi=\frac{C}{(T-T_c)} , \tag{5}$$

where C is proportional to α^{-1} and has units of kelvin; thus, Eq. (4) agrees with Eq. (3b) in this case since the constant β is just $C^{-1}(T_c-T_0)$.

Equations (3a) and (3b) appear to give a good description of the softening of the c_{44} shear elastic constant in the pure cyanides KCN, RbCN, NaCN.[5,6,17] It should be noted, however, that since the full free-energy expansion contains third-order invariants [only invariants up to second order have been included in Eq. (1)], all the phase transitions in question are first order, i.e., a first-order transition occurs at a temperature $T_1>T_c$.[3,11]

In the case of cyanide mixtures, deviations from simple Curie-Weiss behavior are observed at low temperatures.[16–18] The deviations are always observed as enhancements of the elastic constants with respect to what simple Curie-Weiss behavior would give. In order to explain these deviations, Michel[10,11] has introduced the idea of quenched random fields in the mixed cyanides. The source of the random fields is assumed to be the difference in ionic radii of the substitutional ions, which introduces a static distortion of the lattice surrounding each cyanide site. This frozen-in or quenched lattice distortion will vary in a random manner from site to site when the substitutional ions are randomly distributed in the sample. Because of the strong translational-rotational (TR) coupling [large γ in Eq. (1)], these random static strains effectively play the role of conjugate random fields acting on the pseudospins, which in this case are cyanide orientations of quadrupolar symmetry.

We will now include quenched random fields in the simple mean-field model by following standard statistical mechanical procedures[19] for quenched random systems. We start out with a mean-field Hamiltonian of the form

$$H=-\sum_i(zJ_{\rm eff}Y+h_u+h_i)Y_i . \tag{6}$$

Here Y_i is the cyanide orientational pseudospin of quadrupolar symmetry at site i, Y is the corresponding macroscopic order parameter that appears in Eq. (1), z is the CN^--CN^- coordination number, $J_{\rm eff}$ is the effective CN^--CN^- coupling constant corresponding to the parameter T_c in Eq. (5), [$kT_c=zJ_{\rm eff}$], h_u is a uniform external field (in energy units) conjugate to Y, and h_i is a site-dependent random field. The term random field means that $[h_i]_{\rm av}=0$ while $[h_i^2]_{\rm av}\equiv\Delta\neq0$, where $[\ ]_{\rm av}$ denotes the sample average; i.e., for a quantity X that depends on h_i

$$[X(h_i)]_{\rm av}=\int_{-\infty}^{\infty}p(h_i)X(h_i)dh_i , \tag{7}$$

where $p(h_i)$ is the random-field probability distribution. We can now calculate the free-energy per spin

$$F=-\frac{kT}{N}\left[\ln\sum_{\{Y_i\}}e^{-H/kT}\right]_{\rm av}=-\frac{kT}{N}[\ln Z_i]_{\rm av} \tag{8}$$

and the equation of state

$$Y=-\frac{\partial F}{\partial h_u}=[\langle Y_i\rangle_T]_{\rm av}=[g(h_{\rm eff}/kT)]_{\rm av} , \tag{9}$$

where

$$\langle Y_i\rangle_T=\frac{1}{Z_i}\sum_{\{Y_i\}}Y_ie^{-H/kT}$$

denotes the thermal average of Y_i for a given h_i

configuration, and the effective field is given by

$$h_{\text{eff}}=zJ_{\text{eff}}Y+h_u+h_i \ . \tag{10}$$

As an example, one may follow this procedure and easily find the equation of state for the Ising model ($Y_i=\pm 1$):

$$Y=\left[\tanh\left[\frac{zJ_{\text{eff}}Y+h_u+h_i}{kT}\right]\right]_{\text{av}} . \tag{11}$$

In the present case we are only interested in the high-temperature cubic phase of the cyanides, i.e., $Y=0$. We work further under conditions where the external uniform field is equal to zero, i.e., $h_u=0$. Thus,, to calculate the order-parameter susceptibility we may expand the equation of state Eq. (9) in small values of Y and h_u, and keep only linear terms;

$$Y=\frac{1}{kT}(zJ_{\text{eff}}Y+h_u)[g'(h_i/kT)]_{\text{av}} , \tag{12}$$

where $g'(y)=dg(y)/dy$. Taking the derivative of Y with respect to the field yields $\chi=\partial Y/\partial H_u$, where $H_u=Dh_u$ is the (dimensionless) uniform field conjugate to Y and D is a conversion constant with dimensions of inverse energy. Thus, we find

$$\chi=\frac{1}{Dk}\frac{[g'(h_i/kT)]_{\text{av}}}{T-T_c[g'(h_i/kT)]_{\text{av}}} . \tag{13}$$

This expression replaces the order-parameter susceptibility given in Eq. (5) when random fields are included in the analysis. Note that $1/Dk$ corresponds to the Curie constant C in Eq. (5).

We now define the Edwards-Anderson order parameter

$$q\equiv[\langle Y_i\rangle_T^2]_{\text{av}}=\left[\left[g\left[\frac{h_i}{kT}\right]\right]^2\right]_{\text{av}} \tag{14}$$

and make the following observations.

(i) In the case of the Ising model, $g(h_i/kT)=\tanh(h_i/kT)$; thus, $g'(h_i/kT)=1-(g(h_i/kT))^2$ and $[g'(h_i/kT)]_{\text{av}}=1-q_I$. As a result,

$$\chi=\chi_{\text{Ising}}=\frac{C(1-q_I)}{T-T_c(1-q_I)} , \tag{15}$$

with $q_I=[\tanh^2(h_i/kT)]_{\text{av}}$. Equation (15) was derived earlier by Schneider and Pytte[20] applying the replica trick.

(ii) In the general case, one can expand χ and q in terms of the small quantity h_i/kT provided that the energy scale is set by kT, or in other words the random-field distribution width σ is much smaller than kT. If this is the case, one can easily show that

$$\chi=\frac{C[1+\frac{1}{2}g'''(0)q]}{T-T_c[1+\frac{1}{2}g'''(0)q]}\simeq\frac{C(1-q)}{T-T_c(1-q)} , \tag{16}$$

and

$$q\simeq\frac{[h_i^2]_{\text{av}}}{k^2T^2}=\frac{\Delta}{k^2T^2}\simeq\frac{\sigma^2}{k^2T^2} , \tag{17}$$

where we have used $g'(0)=1$, which follows from Eqs. (5) and (13), and have made use of $[h_i]_{\text{av}}\equiv 0$. We have also taken $g'''(0)=-2$ as for the Ising model. Thus, the simple expression on the right-hand side in Eq. (16) is valid except possibly for a multiplicative factor $[-g'''(0)/2]$ of order of magnitude 1 in front of q. In the Ising case, this factor is exactly 1. Substituting this result for χ into Eq. (4) we find

$$\frac{c_{44}}{c_{44}^0}=\frac{s_{44}^0}{s_{44}}=\frac{T-T_c(1-q)}{T-T_0(1-q)}=\frac{T-T_c(1-\Sigma/T^2)}{T-T_0(1-\Sigma/T^2)} , \tag{18}$$

where

$$\Sigma\equiv qT^2=\frac{\Delta}{k^2} . \tag{19}$$

Equation (18) represents the main result of our mean-field analysis, and will be applied in the data analysis below. This equation appears to describe the temperature dependence of the elastic constants in mixed cyanides well. In the pure systems (KCN, RbCN, NaCN, etc.), the quenched random fields h_i, and thus, the Edwards-Anderson order-parameter q are zero, and Eq. (18) is identical to the pure Curie-Weiss behavior given in Eq. (3b). In cyanide mixtures where nonzero random fields are believed to be present due to the difference in ionic radii of the substitutional ions, $q\neq 0$, and Eq. (18) will give higher values of the elastic constants compared to the pure $q=0$ Curie-Weiss law.

We have defined the Edwards-Anderson order-parameter q here in analogy with spin-glass terminology. Our q and the spin-glass order parameter are by definition the same thermodynamic quantities. In the present case, however, there is a nonzero random-field-induced q present at all temperatures [q falls off as $1/T^2$ at high temperatures according to Eq. (17)]. In the spin-glass case there is a random-exchange-induced q (i.e., $[J_{ij}]_{\text{av}}=0$ but $[J_{ij}^2]_{\text{av}}\neq 0$), which is nonzero only below the thermodynamic spin-glass transition. One might extend the present model and include nonzero random exchange in addition to the quenched random fields. The effect of random exchange could presumably also be treated within mean-field theory. This would correspond to a Sherrington-Kirkpatrick model[21] with the addition of a random field. By expanding the free energy, Eq. (8), in small random fields, one may easily show that $\Delta=[h_i^2]_{\text{av}}$ is the field conjugate to the Edwards-Anderson order-parameter $q=[\langle Y_i\rangle^2]_{\text{av}}$.[19] Thus, a model with both nonzero random exchange and nonzero quenched random field would correspond to a spin-glass transition in a nonzero external conjugate field. Since the effective CN^--CN^- pseudospin exchange interaction is strongly angle dependent, there is a real possibility of a random component in the effective coupling constant J_{eff}.[22] This would induce spin-glass-like ordering or spin-glass-like dynamics in the cyanide mixtures. Important precursor effects however, will result from the nonzero quenched random fields even in the absence of random exchange. At high temperatures, it can be shown that the presence of random exchange interactions would transform Eq. (17) into

$$q \simeq \frac{\sigma^2}{(kT)^2}\left[1+\frac{\sigma_J^2}{(kT)^2}\right], \tag{20}$$

where σ_J is the width of the quenched random-exchange interaction distribution. We will return to these possibilities during subsequent data analysis.

According to our mean-field model the quantities T_0 and T_c are proportional to the coordination number z. In mixtures like $K_xRb_{1-x}CN$ and $K_xNa_{1-x}CN$, $z=12$ is constant. In the diluted systems like $K(CN)_xBr_{1-x}$ and $RbCN_xBr_{1-x}$, $z=12x$ provided the mixing is random.

It is clear that the random fields $\Delta=[h_i^2]_{\rm av}$ as discussed here will be zero for pure samples ($x=0$ and 1). In the diluted cyanides the nonspherical cyanide ions are being replaced by spherical ions (bromide or chloride). Michel[10,11] has argued that the asphericity can be neglected and that Δ is proportional to $x(1-x)$ in diluted cyanide mixtures.

Assuming that one can neglect the effects of random exchange and aspherical cyanide ions and assuming random mixing, we may thus write

$$\frac{c_{44}}{c_{44}^0}=\frac{s_{44}^0}{s_{44}}=\frac{T-T_c(x)[1-x(1-x)\Sigma_0/T^2]}{T-T_0(x)[1-x(1-x)\Sigma_0/T^2]}, \tag{21}$$

where $T_c(x)=xT_{c1}$ and $T_0(x)=xT_{01}$ in the case of diluted cyanides [$T_{c1}\equiv T_c(x=1)$ and $T_{01}\equiv T_0(x=1)$].

Equation (21) is identical to the result of Michel, with the following parameter mapping:

$$T_{c1}\equiv T_{01}+\frac{\gamma^2}{\alpha}s_{44}^0=T_{01}+\frac{2B^2}{a}s_{44}^0 y_w , \tag{22a}$$

$$T_{01}=(-J-C^s)y_w , \tag{22b}$$

$$\Sigma_0=\xi_w h^2 , \tag{22c}$$

where B, a, y_w, J, C^s, ξ_w, and h are as defined by Michel.[11]

As a function of temperature, Eq. (21) is always going to give a minimum in c_{44}. Above the critical composition, x_c, in diluted cyanide mixtures, however, this minimum occurs for a negative c_{44} value. Thus, in this case the lattice-mediated CN^--CN^- coupling is strong enough, compared to the width of the random quenched field distribution, to induce the simultaneous ordering of the quadrupolar lattice and cyanide orientational degrees of freedom. For compositions $x<x_c$ on the other hand, c_{44} will never reach zero because the randomly distributed variations in the cyanide-ion local potentials are too large to enable the effective CN^--CN^- interaction to induce quadrupolar order. Differentiating Eq. (18) with respect to T, we find that a minimum in c_{44} will occur at a temperature T_f given by

$$T_f=(3\Sigma)^{1/2} \text{ or } q_f=\tfrac{1}{3} . \tag{23}$$

Inserting this result back into Eq. (18) we identify the critical composition x_c from the criterion that $c_{44}=0$ at $T_f(x_c)$:

$$T_f(x_c)-T_c(x_c)(1-q_f)=0 . \tag{24}$$

Using

$$T_f(x_c)=[3x_c(1-x_c)\Sigma_0]^{1/2} ,$$

$T_c(x_c)=x_cT_{c1}$ and $q_f=\frac{1}{3}$, we find

$$x_c \simeq \frac{\Sigma_0}{\Sigma_0+\frac{4}{27}T_{c1}^2} , \tag{25}$$

as a crude approximate result.

In the analysis above we have followed Michel[10,11] and others[20] and used a high-temperature expansion for the Edwards-Anderson order-parameter $q\simeq\Sigma/T^2$. This approximation is obviously going to break down for temperatures below which Σ/T^2 becomes larger than 1 since $q<1$ by definition. In Sec. IV, some of the data to be analyzed lie in a temperature region where $\Sigma/T^2>1$. In this case, a low-temperature expansion rather than a high-temperature expansion should be used. Assuming a symmetric random-field distribution, the following expansion in small values of kT/σ is a straightforward exercise[23]

$$[g'(h_i/kT)]_{\rm av}\simeq A_0\frac{kT}{\sigma}+B_0\left[\frac{kT}{\sigma}\right]^3 + \text{higher-order terms} , \tag{26}$$

where σ is the quenched random-field distribution width as before and A_0 and B_0 are constants. Thus, at low temperatures the quantity $(1-q)$ in Eqs. (16) and (18) should be replaced by

$$(1-q)\simeq A\frac{T}{\Sigma^{1/2}}+B\frac{T^3}{\Sigma^{3/2}}+\text{higher-order terms} , \tag{27}$$

where A and B are constants of order of magnitude 1. These results could also have been obtained by expanding Eq. (14) in the same parameter. Here we have neglected possible random interactions, which could trigger a spin-glass transition, accompanied by an additional spontaneous component in q. Recently, Michel has argued[24] that a nonergodic instability should lead to an additional contribution to q at low temperatures. Thus, low-temperature forms other than Eqs. (26) and (27) may have to be considered in a complete treatment of data at $T<T_f$. As discussed by Michel,[10,11] quantum effects might also have to be considered at low temperatures.

III. EXPERIMENTAL PROCEDURE AND RESULTS

Single crystals of $Rb(CN)_xBr_{1-x}$ obtained from Lüty were grown from the melt at the Crystal Growth Laboratory of the University of Utah. The oriented samples studied were thin slabs ($1\times1\times0.25$ cm^3) cleaved from large single crystals. Terraces on the (100) surfaces were polished away to give surface roughness and nonparallelity less than 1 μm, which is much smaller than the smallest wavelength $\lambda\simeq30$ μm ($\lambda=v/f$, where $v\simeq300$ m/s is the smallest measured velocity and $f\simeq10$ MHz for all the runs analyzed here).

Point defects surrounded by strains could be observed in some of the samples when they were placed between crossed polarizers and viewed with a microscope. For-

TABLE I. Gases used as acoustic bonding materials. bp and fp are boiling and freezing points, respectively.

Gas	fp (K)	bp (K)
Ne	24.48	27.10
N_2	63.29	77.35
Ar	83.95	87.45
Xe	161.2	166.1
CCl_2F_2 (Freon 12)	115.0	246.9
$C_2Cl_2F_4$ (Freon 114)	179.0	276.8

tunately, the homogeneous regions between these point-like strain sources were large enough to allow application of an ultrasonic transducer with an active diameter of ~ 3.5 mm.

In these experiments we used overtone polished lithium niobate ultrasonic transducers with a fundamental frequency $f_0 \simeq 10$ MHz to generate and detect transverse acoustic waves propagating in the [100] direction. Due to the difference in thermal expansion between the transducer and the sample, sample cracking occurred frequently on slow cooling at temperatures 50–60 K below the freezing point of the acoustic bond used between the transducer and the sample. In order to avoid cracking the sample, we applied the bonding technique previously used in experiments on $K(CN)_xBr_{1-x}$ mixtures by Feile *et al.*,[16] who used gases with low boiling and freezing points as bonding materials. Our sample holder was designed so that gases could be condensed onto or evaporated from the sample surface at low temperatures during the course of the experiment. The materials used as bonds for the present experiments are listed in Table I. At temperatures between room temperature and 180 K, Dow-Corning 200 silicone fluid or phenyl salicylate were used. Due to the limited temperature range over which any single bonding material could be used, the low-temperature experiments were carried out as a series of several temperature cycles in order to enable changes of acoustic bonds.

The standard flotation method was used to determine the room temperature density ρ of the samples. A linear interpolation between the densities of pure RbCN and pure RbBr was then used to determine sample compositions,[6,25] giving x values different from the nominal (melt) compositions in all cases, as shown in Table II.

During each run, the absolute sound velocity v was measured every 50–100 K with an estimated accuracy of better than $\pm 1\%$ using the Papadakis pulse overlap technique.[26] The resulting room-temperature elastic constants $c_{44}(300\text{ K}) = \rho(300\text{ K})\, v^2(300\text{ K})$ are shown in Table II. Relative changes in sound velocities as a function of temperature were detected with an estimated precision of $\pm 10^{-3}\%$ using a computerized phase-sensitive MATEC MBS 8000 system.[27] However, several runs were made for each composition. Different runs sometimes involved different regions of a given crystal or different crystals cut from a single large sample, and there may be small concentration gradients in these melt-grown samples. As a result, the overall scatter in the velocity data for a given composition is about $\pm 0.1\%$. Cooling and warming runs were reproducible in all cases.

A liquid-nitrogen cryostat was used in the experiments for temperatures above 80 K. In this case the temperature of the sample was controlled by means of a manually set Bailey temperature controller. The temperature was stabilized at each data point for 20–30 min and measured with a calibrated platinum resistance thermometer to an accuracy of ± 2 mK. At temperatures below 80 K (or higher for some of the runs), a continuous-flow liquid-helium Janis Supertran Cryostat was used. In this case the temperature was seldom held constant but was allowed to drift *slowly* with a scanning rate set according to the temperature region being investigated. In all cases both cooling and heating runs were made in order to ensure that the scanning rate was sufficiently slow. The scanning rate could be as high as 15 K/h at high temperatures and in most cases was less than 2 K/h in temperature regions with high anomalous sound attenuation. The scanning rate was set by adjusting the liquid-helium flow combined with a Lakeshore model DRC 81C tem-

TABLE II. $Rb(CN)_xBr_{1-x}$ sample properties. x and x_{nom} are the measured and nominal sample compositions, respectively. ρ is the density determined by the flotation method. $c_{44}(300\text{ K})$ in units of 10^9 N/m^2 or 10^{10} dyn/cm^2 is the static-shear elastic constant at $T = 300$ K determined with an absolute accuracy of $\pm 1.5\%$. The estimated random error in the c_{44} data for a given composition is given by the standard deviation σ (in units of 10^9 N/m^2). T_l is the temperature at which the acoustic signal was lost on cooling and $c_{44}(T_l)$ (in units of 10^9 N/m^2) is the value of the elastic constant at $T = T_l$.

Analyzed x	Nominal x_{nom}	ρ (g/cm^3)	$c_{44}(300\text{ K})$	σ	T_l (K)	$c_{44}(T_l)$
	0(RbBr)	3.355	3.761			
0.06	0.1	3.290	3.562	0.006	13.11	1.73
0.19	0.2	3.156	3.098	0.006	32.24	1.14
0.25	0.3	3.101	2.886	0.006	39.32	0.923
0.44	0.5	2.904	2.585	0.005	57.48	0.452
0.53	0.6	2.813	2.325	0.0045	63.49	0.270
0.67	0.7	2.666	2.067	0.004	78.45	0.129
0.79	0.8	2.549	1.908	0.004	89.02	0.0836
0.87	0.9	2.464	1.795	0.0018	105.3	0.167
	1(RbCN)	2.328	1.652	0.004	133.0	0.213

perature controller. Below 80 K a calibrated silicone-diode thermometer enabled temperature readings to be made with an accuracy of ± 10 mK, whereas at temperatures above 80 K the platinum resistance thermometer was used.

Elastic constants $c_{44}=\rho v^2$ are shown as a function of temperature in Fig. 1. RbBr ($x=0$) and RbCN ($x=1$) elastic constant data have been taken from the literature.[6,25] Since both sample thicknesses and densities were measured at room temperature, all the data were corrected for thermal expansion effects. A linear interpolation between the thermal expansion coefficients, α, for pure RbCN ($\alpha \simeq 6\times 10^{-5}$ K^{-1}) (Ref. 4,6) and pure RbBr ($\alpha \simeq 1.4\times 10^{-5}$ K^{-1}) (Ref. 28) was used. The smooth curves in Fig. 1 represent theoretical fits to the data as described below.

For all the samples, the sound attenuation stayed moderate and constant ($\simeq 10$ dB/cm) from room temperature down to 10–20 K (depending on the measuring frequency) above the temperature where the acoustic signal was lost due to high sound absorption. A detailed discussion of the attenuation data will be presented elsewhere.[29] Here we will only mention that the attenuation scales as the frequency squared over the range from 8 to 77 MHz, indicating relaxational attenuation rather than elastic scattering as the cause of signal loss. Indeed, the analysis of the attenuation data shows that $\omega\tau \ll 1$, where τ represents an effective average relaxation time. This is in complete agreement with the fact that no dispersion was observed in the sound velocity. This absence of velocity dispersion is illustrated in Fig. 2, which shows in more detail c_{44} data for the samples with $x=0.19$ and 0.25. Thus, we believe that all the data presented in Figs. 1 and 2 represent *static* elastic constants $c_{44}=\rho v^2(\omega=0)$.

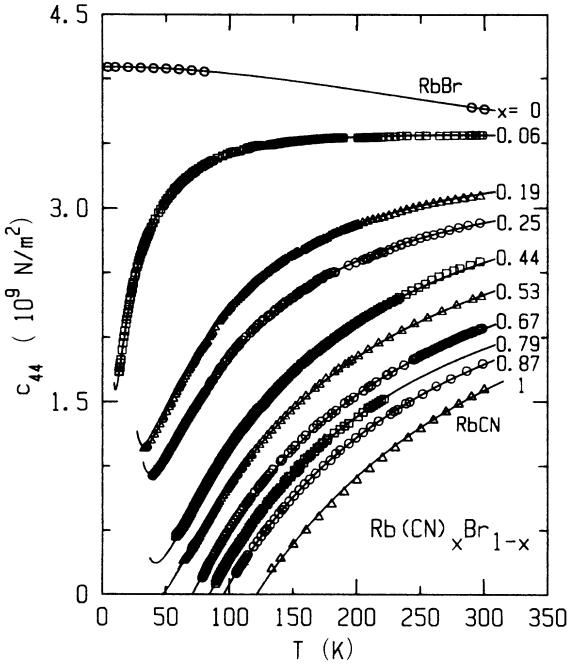

FIG. 1. Temperature dependence of the static c_{44} elastic constant in Rb(CN)$_x$Br$_{1-x}$ single crystals. Data on RbBr and RbCN are taken from Refs. 24 and 6, respectively. The smooth curves represent random-field fits with Eqs. (18), (28), and (29) as described in the text.

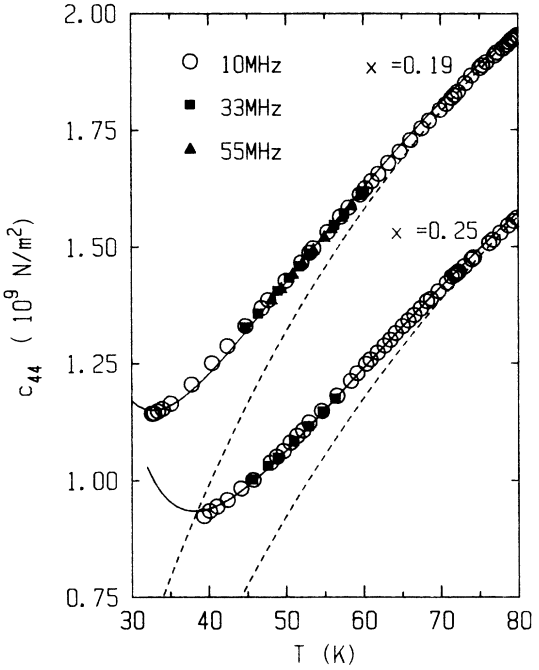

FIG. 2. Detailed view of the temperature dependence of c_{44} in two Rb(CN)$_x$Br$_{1-x}$ crystals at several ultrasonic frequencies. The solid curves are random-field fits identical to those shown in Fig. 1; the dashed curves are truncated Curie-Weiss fits discussed in Sec. IV.

For one sample ($x=0.19$), it is possible to recover the acoustic signal at low temperatures ($T<15$ K), as shown in Fig. 3. Due to the small signal amplitude it was only possible to obtain data below 15 K at the lowest frequen-

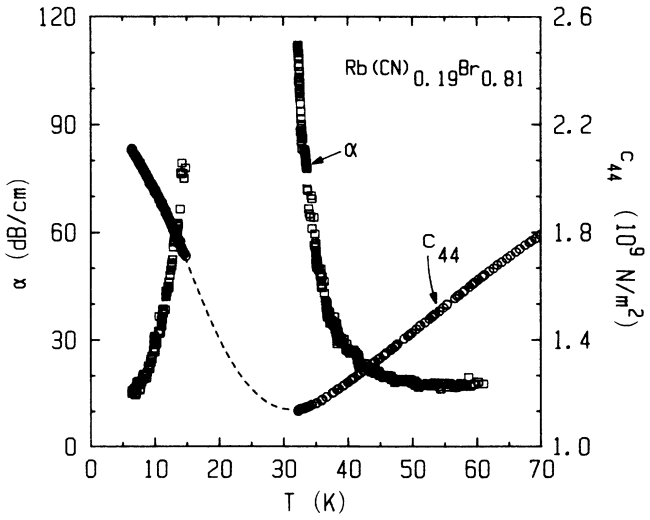

FIG. 3. Temperature dependence of the static elastic constant, $c_{44}=\rho v^2$, and sound attenuation α for the TA [100] mode in a Rb(CN)$_{0.19}$Br$_{0.81}$ single crystal. These measurements were made at 8–9 MHz. The dashed line is a guide for the eye.

cy (9 MHz). The low-temperature data shown in Fig. 3 represent two warming and one cooling run, each run carried out at different but slow (<5 K/h) scanning rates. No hysteresis was seen. In one case, the system was stabilized at 10.00 ± 0.01 K for 2 h. No long-time drift in ultrasonic attenuation or velocity was observed during these 2 h.

IV. DATA ANALYSIS AND DISCUSSION

We have fitted the static elastic constant data shown in Fig. 1 with Eq. (18). The effect of lattice anharmonicity has been included by replacing the constant parameter c_{44}^0 in Eq. (18) with a temperature-dependent bare elastic constant given by[16]

$$c_{44}^0(T)=c_{44}^0\left[1+\alpha_{44}\frac{\Theta_D}{e^{\Theta_D/T}-1}\right], \tag{28}$$

where α_{44} is a negative constant of the order of magnitude of 10^{-4} K^{-1} and Θ_D is the Debye temperature. In all the fits we have used $\Theta_D=136.5$ K, the Debye temperature for pure RbBr.[30] Taking Eq. (22a) into account, the parameter T_c in Eq. (18) has been replaced by

$$T_c(T)=T_0+(T_c-T_0)\frac{c_{44}^0(T_c)}{c_{44}^0(T)}$$

$$=T_c+(T_c-T_0)\frac{c_{44}^0(T_c)-c_{44}^0(T)}{c_{44}^0(T)}\ . \tag{29}$$

Equation (29) has been included in the present analysis although it only represents a very small correction to the value of T_c. For the present data, Eq. (29) gives at most a 3% variation over the entire temperature range. Parameters from our fits to all the experimental data are summarized in Table III, and the composition dependence of the parameters c_{44}^0, T_c, T_0, and Σ is shown in Figs. 4–7.

We will now discuss these fits. For x values less than 0.6, the fits converge with positive Σ values when all five parameters c_{44}^0, α_{44}, T_c, T_0, and Σ are allowed to be freely adjustable quantities. These random-field parameters are presented by filled circles in Figs. 4–7. For these compositions ($x<0.6$), c_{44} exhibits a point of inflection at a temperature $T_i>T_l$ where T_l values are given in Table II. Thus, for these samples satisfactory Curie-Weiss fits, i.e., $\Sigma=0$ in Eq. (28), can only be achieved by ignoring data points at low temperatures. As an example, such truncated Curie-Weiss fits were carried out for the $x=0.19$ and 0.25 crystals with fitting ranges 67–300 K and 77–300 K, respectively. The resulting fitting parameters are $c_{44}^0=3.929\times10^9$ N/m^2, $\alpha_{44}=-1.5\times10^{-4}$ K^{-1}, $T_c=20.0$ K, and $T_0=-38.0$ K for the $x=0.19$ sample and $c_{44}^0=3.896\times10^9$ N/m^2, $\alpha_{44}=-1.4\times10^{-4}$ K^{-1}, $T_c=24.7$ K, and $T_0=-56.1$ K for the $x=0.25$ sample. The truncated Curie-Weiss fits are indistinguishable from the random-field fits listed in Table III over the temperature range 80K–300 K. However, as shown in Fig. 2, the discrepancies between the data points and the truncated Curie-Weiss fits at temperatures below 80 K are fully accounted for by the random-field fits. Thus for all samples with $x<0.6$, random field fits with $\Sigma>0$ are superior to Curie-Weiss fits for describing the entire temperature range between T_l and 300 K.

For mixed crystal samples with x larger than 0.6, the free fits converge to give Σ values that are rather small and uncertain positive values ($+140\pm160$ for $x=0.79$) or negative values (-1325 ± 800 for both $x=0.67$ and 0.87). We then carried out fits with Σ fixed at zero, which gave the fit parameters represented by open circles in Figs. 4–6. The latter fits, which correspond to traditional Curie-Weiss behavior, give T_c and Σ values that are inconsistent with the expected trend based on the $x<0.6$ parameters. We have therefore, adopted the $x(1-x)$ behavior for Σ suggested by Michel and made

TABLE III. Values of adjustable parameters c_{44}^0 (the bare elastic constant at 0 K in units of 10^9 N/m^2 or 10^{10} dyn/cm^2), α_{44} (in units of 10^{-4} K^{-1}), T_c, T_0, and Σ appearing in Eqs. (18) and (28). χ_ν^2 represent reduced chi-squared values resulting from Curie-Weiss (CW; i.e., $\Sigma=0$) fits and random-field (RF) fits as described in the text. Quantities in parentheses were held fixed at the values indicated. In RbBr where there are no random fields and no cyanide pseudospins present, the parameters result from a Debye anharmonic (DA) fit of data from Ref. 24 using Eq. (28).

x	Fit	c_{44}^0	α_{44}	T_c (K)	T_0 (K)	Σ (K^2)	Goodness of fit χ_ν^2
0.0	DA	4.086	−3.4	0.0	0.0	0	
0.06	RF	3.835	−1.5	7.3	−3.6	33	1.0
0.19	RF	3.965	−1.5	24.5	−35.5	355	1.9
0.25	RF	3.910	−1.4	32.1	−47.8	482	1.4
0.44	RF	4.090	−1.0	54.1	−77.0	573	1.4
0.53	RF	3.957	−1.0	63.8	−86.5	579	2.3
0.67	CW	4.126	−1.6	71.4	−123.5	(0)	1.1
	RF	3.998	−1.6	78.6	−100.3	(512)	1.9
0.79	CW	3.983	−2.0	84.4	−111.7	(0)	1.6
	RF	3.906	−2.0	89.2	−96.3	(384)	1.7
0.87	CW	3.958	−1.5	95.3	−121.4	(0)	0.78
	RF	3.894	−1.5	98.1	−110.7	(262)	0.91
1.0	CW	4.251	−1.5	121.19	−143.2	(0)	12.6

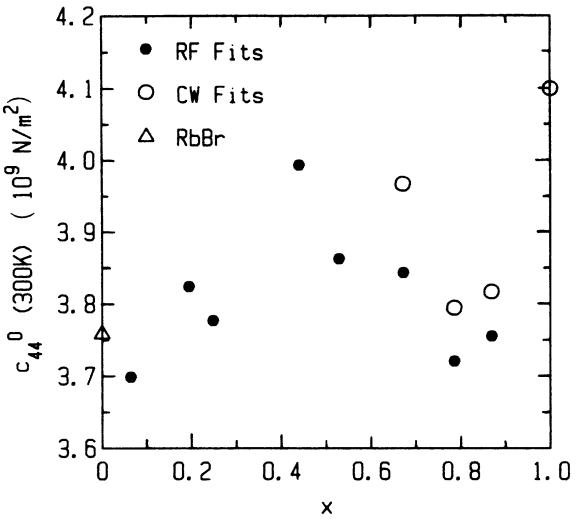

FIG. 4. Composition (x) dependence of the bare elastic constant $c_{44}^0(300\ \mathrm{K})$ determined from fitting the data shown in Fig. 1 to Eqs. (18), (28), and (29). Parameters resulting from both Curie-Weiss (CW) and random-field (RF) fits as described in the text are shown.

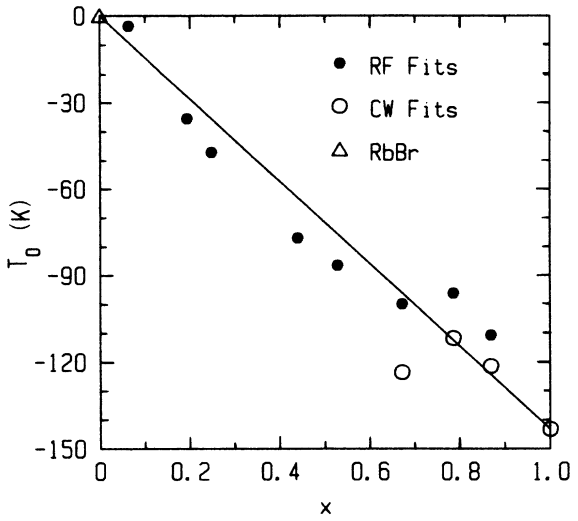

FIG. 6. Composition (x) dependence of the fitting parameter T_0. The mean-field percolation prediction is represented by the straight line. CW and RF denote Curie-Weiss and random-field fits, respectively.

such a fit to the Σ values for the $x<0.6$ samples. This fit yields the parabolic line shown in Fig. 7. We have then used this line to determine the Σ parameter for the three mixed crystals with $x>0.6$. The c_{44} fits achieved for these three samples with fixed nonzero Σ values are equivalent to all the other fits when residual plots or reduced χ_ν^2 values are compared (see Table III).[31] The parameters from such random field fits are represented by solid circles in Figs. 4–6. Since the simple Curie-Weiss fits give parameters that are physically less plausible, we believe that the apparent statistical acceptability of Curie-Weiss behavior for samples with $1>x>0.6$ is an artifact of high T_l values and consequently small Σ/T^2 values in the accessible temperature range (see Table IV). Therefore, the parameters shown as solid circles in Figs. 4–6, and the corresponding random-field fit curves drawn in Fig. 1, provide the best representation of the present data on the static c_{44} elastic constants of $Rb(CN)_xBr_{1-x}$ mixed crystals.

All the parameters show x dependences in very good agreement with the predictions summarized in Sec. II. Thus, the present data confirm the validity of Michel's quenched random-field picture for this mixed cyanide sys-

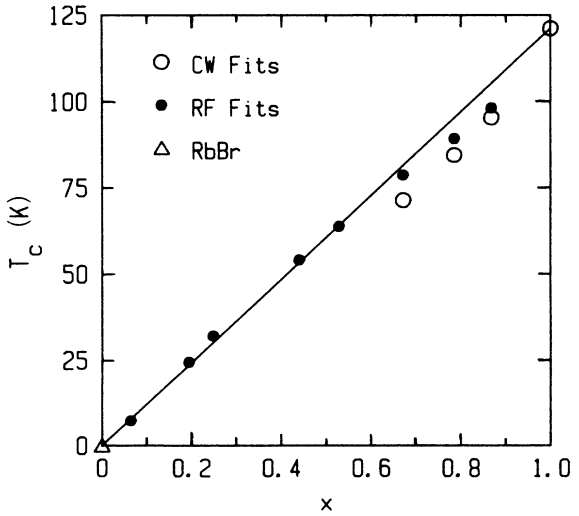

FIG. 5. Composition (x) dependence of the quadrupolar ordering temperature T_c. The straight line represents the mean-field percolation prediction. Both Curie-Weiss (CW) and random-field (RF) fits, as discussed in the text, are shown.

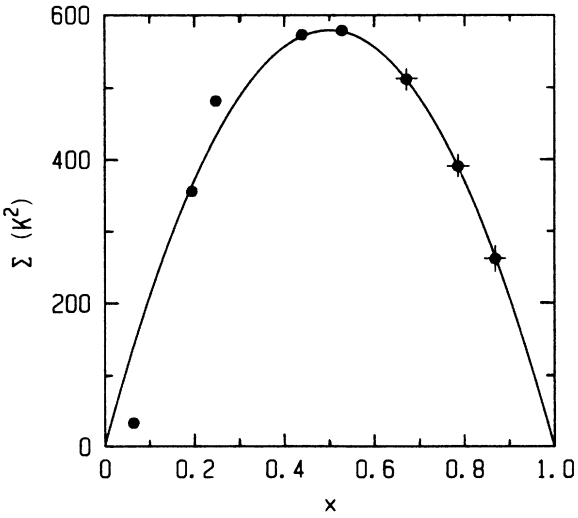

FIG. 7. Composition (x) dependence of the fitting parameter Σ, which is proportional to the square of the quenched random-field distribution width. The parabolic line represents a fit of the form $\Sigma=\Sigma_0 x(1-x)$ to data for $x<0.6$; the resulting $\Sigma_0=2317\ \mathrm{K}^2$. The points-◆-for samples with $x>0.6$ are smooth curve values that were adopted for the RF fits (see Table III).

TABLE IV. Values of the cubic lattice parameter a and the quantities $c_{44}^0(300\ \text{K})$, given in units of $10^9\ \text{N/m}^2$, $a^4c_{44}^0(300\ \text{K})$ (in units of $10^{-28}\ \text{N m}^2$, Σ/T_l^2, and T_f. $c_{44}^0(300\ \text{K})$ has been calculated from Eq. (28). Σ/T_l^2 (T_l is given in Table II) represent the largest values of the high-temperature expansion parameter Σ/T^2. T_f are the temperatures at which c_{44}, as given by Eq. (18) with the fit parameters in Table III, has a minimum for positive c_{44} or goes to zero.

x	a (nm)	$c_{44}^0(300\ \text{K})$	$a^4c_{44}^0(300\ \text{K})$	Σ/T_l^2	T_f (K)
0.0	0.6892	3.761	8.49		
0.06	0.6889	3.699	8.33	0.19	9.98[a]
0.19	0.6882	3.824	8.58	0.35	32.6[a]
0.25	0.6879	3.777	8.46	0.32	38.0[a]
0.44	0.6869	3.993	8.89	0.18	41.5[a]
0.53	0.6864	3.863	8.58	0.15	47.0[b]
0.67	0.6857	3.844	8.50	0.083	70.5[b]
0.79	0.6851	3.721	8.20	0.049	84.1[b]
0.87	0.6847	3.756	8.26	0.024	95.2[b]
1.0	0.6840	4.100	8.97		

[a]A minimum for positive c_{44}.
[b]Goes to zero.

tem,[10,11] at least for temperatures where the high-temperature expansion is valid.

In Table IV we have calculated the quantities $a^4c_{44}^0(300\ \text{K})$, where a is the cubic lattice constant determined from a linear interpolation between the RbBr and RbCN values. This quantity has a universal value for all univalent crystals of the rocksalt structure according to rigid-ion models, and this is still a good approximation empirically and according to simple shell models.[15] We have calculated this quantity for several alkali-metal halide crystals[28] (KBr, KCl, KF, KI, RbCl, RbF, RbI, $KCl_{0.75}Br_{0.25}$, $KCl_{0.4}Br_{0.6}$, and $KCl_{0.25}Br_{0.75}$), obtaining $a^4c_{44}^0(300\ \text{K})$ values ranging from $8.5\times10^{-28}\ \text{N m}^2$ to $10.0\times10^{-28}\ \text{N m}^2$. Our $Rb(CN)_xBr_{1-x}$ values are in excellent agreement with this empirical range.

The c_{44} data for pure RbCN, which were taken from Ref. 6, exhibited significant and systematic (roughly sinusoidal) deviations from any theoretical fit curve over the entire temperature range. Also the bare stiffness c_{44}^0 obtained from the least-squares Curie-Weiss fit was unexpectedly large ($4.7\times10^9\ \text{N/m}^2$ compared with the range 3.8×10^9 to 4.1×10^9 for the other nine samples). It is quite likely that there is some systematic error in these RbCN data, which would not be surprising in view of the lower purity and lesser crystal perfection of the best samples of RbCN grown eight years ago.[13] Furthermore, the uncertainty cited by Haussuhl is fairly large ($\pm3\%$). We have systematically adjusted the RbCN c_{44} values by multiplying each reported $c_{44}(T)$ by the constant factor 0.97. The Curie-Weiss fit reported in Table III corresponds to this adjusted data set. The resulting bare stiffness c_{44}^0 is then $4.25\times10^9\ \text{N/m}^2$, in better agreement with our mixed crystal results, and the values of T_c, T_0, and c_{44}^0 (300 K) also fit in well with the overall trends for these parameters.

The fit to $\Sigma(x)$ shown in Fig. 7 yields $\Sigma_0=2317$ for the random-field distribution width strength for the present system. Inserting this result into Eq. (25) we find $x_c\simeq0.52$, which is consistent with the present experimental observations and with optical transmission studies.[13] Thus, the present data analysis is self-consistent.

We have analyzed previously[14] the low-temperature data for the $Rb(CN)_{0.19}Br_{0.81}$ sample (shown in Fig. 3), in terms of the low-temperature expansion given in Eq. (27). The fits to the $Rb(CN)_{0.19}Br_{0.81}$ data are shown in Fig. 8 where we have plotted the Edwards-Anderson order parameter q calculated from

$$q=1-T\frac{(c_{44}/c_{44}^0-1)}{(T_0c_{44}/c_{44}^0-T_c)}\ , \tag{30}$$

which follows from Eq. (18). The value of q falls off as

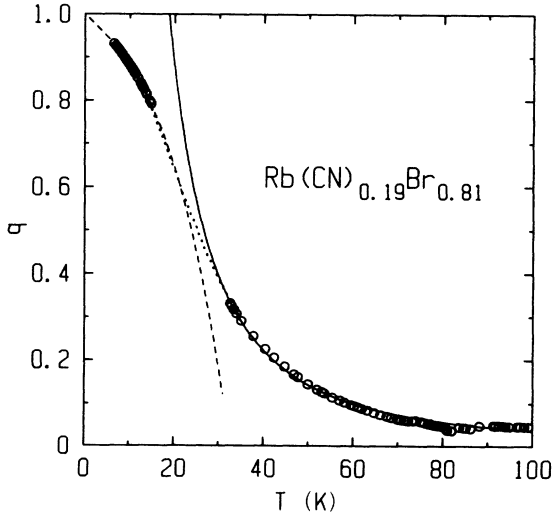

FIG. 8. The Edwards-Anderson order-parameter q as calculated from Eq. (30) with parameters given in Table III, for the $Rb(CN)_{0.19}Br_{0.81}$ data. The high-temperature curve (solid line) represents Σ/T^2 with $\Sigma=355\ \text{K}^2$; while the low-temperature q data were fitted to Eq. (27) (dashed line). The dotted line, which is merely a guide for the eye, represents a smooth interpolation between the high- and low-temperature data sets. See also Ref. 14.

$1/T^2$ at high temperatures and approaches 1 at low temperatures. The low-temperature expansion fit to q with Eq. (27) yields parameters $A=0.19$ and $B=0.13$, which are in reasonable agreement with what general theoretical estimates would suggest ($A \simeq B \simeq 1$).[23] Thus, within this simple picture there seems to be no need for introducing a spontaneous component in q emerging at low temperatures, suggesting that the quenched random-field picture can be extended beyond the temperature region where the high-temperature expansion fails.

Recently, it has been argued that broken ergodicity might give an additional contribution to q at low temperatures, and that the low-temperature expansions given in Eqs. (26) and (27) are possibly inappropriate.[24] The latter suggestion is especially supported by low-frequency torsion pendulum experiments[7] on $K(CN)_xBr_{1-x}$ crystals. In the case of the present low-temperature data for $x=0.19$ it is not clear which low-temperature form for q is approximate. Furthermore, it remains to be established whether the low-temperature c_{44} elastic constant data for the $x=0.19$ sample represent zero frequency ($\omega\tau \ll 1$) behavior as far as the quadrupolar relaxation is concerned.

V. CONCLUDING REMARKS AND SUMMARY

In conclusion, we have carried out a detailed study of the shear elasticity of $Rb(CN)_xBr_{1-x}$. The static c_{44} elastic constant data show behavior in qualitative agreement with the behavior previously reported for $K(CN)_xBr_{1-x}$ and $K(CN)_xCl_{1-x}$ mixtures.[16–18] We have analyzed our static data with a mean-field model which includes quenched random strain fields. For the high-temperature data we have used a high-temperature expansion for the quenched random-field-induced Edwards-Anderson order-parameter q. The resulting fitting parameters are in excellent agreement with the model predictions presented in Sec. II.

We have thus provided evidence supporting the idea that the orientational freezing process in this system, at least as far as the statics is concerned, can be understood in terms of a competition between quenched random strain fields and the lattice-mediated CN^--CN^- coupling. The present experimental results and analysis support suggestions[10,11,32] that cyanide mixtures should be considered random-field-induced glasses rather than random-interaction-induced frustrated glasses.

A detailed analysis of experimental results on the dynamics of the orientational freezing process will be presented elsewhere.[29] Pretransitional static behavior similar to the one presented here has also been reported for at least one other structural glass system.[33] It would thus be of considerable interest and importance to test the present ideas in other glassy systems and also in crystal systems where imperfection-induced precursor static effects occur close to second-order or weakly first-order structural phase transitions.[34]

ACKNOWLEDGMENTS

This work was supported by the U.S. National Science Foundation under Grant No. DMR-8710035. One of us (J.O.F.) wishes to thank the Royal Norwegian Council for Scientific and Industrial Research (NTNF) for support. We wish to acknowledge F. Lüty for providing single crystal samples and K. Ema for technical assistance during the experiments, and we wish to thank F. Lüty and M. Rowe for many helpful discussions.

[1]F. Lüty, in *Defects in Insulating Crystals*, edited by V. M. Turkevich and K. K. Svarts (Springer-Verlag, Berlin, 1981), p. 69–89.
[2]F. Lüty and J. Ortiz-Lopez, Phys. Rev. Lett. **50**, 1289 (1982).
[3]K. H. Michel and J. M. Rowe, Phys. Rev. B **32**, 5818 (1986); **32**, 5827 (1986).
[4]J. M. Rowe, J. J. Rush, and F. Lüty, Phys. Rev. B **29**, 2168 (1984).
[5]S. Haussuhl, Solid State Commun. **13**, 147 (1973); S. Haussuhl, J. Eckstein, K. Recker, and F. Wallrafen, Acta Crystallogr. Sec. A **33**, 847 (1977).
[6]S. Haussuhl, Solid State Commun. **32**, 181 (1979).
[7]K. Knorr, U. G. Volkmann, and A. Loidl, Phys. Rev. Lett. **57**, 2544 (1986).
[8]T. Shimada, T. Matsuo, H. Suga, and F. Lüty, J. Chem. Phys. **85**, 3530 (1986).
[9]U. G. Volkmann, R. Bohmer, A. Loidl, K. Knorr, U. T. Hochli, and S. Haussuhl, Phys. Rev. Lett. **56**, 1716 (1986).
[10]K. H. Michel, Phys. Rev. Lett. **57**, 2188 (1986).
[11]K. H. Michel, Phys. Rev. B **35**, 1405 (1987); **35**, 1414 (1987).
[12]K. Knorr and A. Loidl, Phys. Rev. B **31**, 5387 (1985).
[13]J. Ortiz-Lopez and F. Lüty, Phys. Rev. B **37**, 5461 (1988); F. Lüty (private communication).
[14]J. O. Fossum and C. W. Garland, Phys. Rev. Lett. **60**, 592 (1988).
[15]K. S. Krishnan and S. K. Roy, Proc. R. Soc. London **210**, 481 (1952); A. D. B. Woods, W. Cochran, and B. N. Brockhouse, Phys. Rev. **119**, 980 (1960); M. J. L. Sangster, J. Phys. Chem. Solids **35**, 195 (1974).
[16]R. Feile, A. Loidl, and K. Knorr, Phys. Rev. B **26**, 6875 (1982).
[17]J. Z. Kwiecien, R. C. Leung, and C. W. Garland, Phys. Rev. B **23**, 4419 (1981).
[18]C. W. Garland, J. Z. Kwiecien, and J. C. Damien, Phys. Rev. B **25**, 5818 (1982).
[19]K. Binder and A. P. Young, Rev. Mod. Phys. **58**, 801 (1986).
[20]T. Schneider and E. Pytte, Phys. Rev. B **15**, 1519 (1977).
[21]S. Kirkpatrick and D. Sherrington, Phys. Rev. B **17**, 4384 (1978).
[22]K. Michel and R. Rowe, Phys. Rev. B **22**, 1417 (1980).
[23]A. Aharony, Phys. Rev. B **18**, 3318 (1978).
[24]K. H. Michel, Z. Phys. B **68**, 259 (1987).
[25]J. T. Lewis, A. Lehoczky, and V. Briscoe, Phys. Rev. **161**, 877 (1967).
[26]E. P. Papadakis, J. Acoust. Soc. Am. **42**, 1045 (1967).
[27]P. W. Wallace and C. W. Garland, Rev. Sci. Instrum. **57**, 3085

(1986).

[28]Landolt and Börnstein, in *Numerical Data and Functional Relationships in Science and Technology*, edited by K.-H. Hellwege (Springer-Verlag, Berlin, 1984), Vol. III.

[29]J. O. Fossum, C. W. Garland, and A. Wells (unpublished).

[30]J. C. Ho and D. P. Dandekar, Phys. Rev. B **30**, 2117 (1984).

[31]In the case of measurements on the $x=0.67$ sample, the Curie-Weiss fit appears to be statistically preferable to the random-field fit. However, in view of the overall trends in the fitting parameters, we feel that the random-field model is physically more reasonable even for this sample.

[32]K. Knorr, E. Civera-Garcia, and A. Loidl, Phys. Rev. B **35**, 4998 (1987).

[33]E. Courtens, F. Huard, and R. Vacher, Phys. Rev. Lett. **55**, 722 (1982).

[34]E. Sandvold, T. Laegreid, K. Fossheim, and J. O. Fossum, Phase Trans. **11**, 145 (1988).